

LINKING PHOTOSYNTHETIC LIGHT USE EFFICIENCY AND OPTICAL VEGETATION ACTIVE INDICATORS: IMPLICATIONS FOR GROSS PRIMARY PRODUCTION ESTIMATION BY REMOTE SENSING

Siheng Wang^{1,*}, Zhen Li¹, Yongguang Zhang^{2,3,4}, Dong Yang¹, Chen Ni¹

¹ Institute of Spacecraft System Engineering, China Academy of Space Technology, Beijing, China – rswangsiheng@163.com; schnappilee@foxmail.com; qbdyzy@sina.com; synichen@163.com

² International Institute for Earth System Sciences, Nanjing University, Nanjing, China - yongguang_zhang@nju.edu.cn

³ Jiangsu Provincial Key Laboratory of Geographic Information Science and Technology, School of Geographic and Oceanographic Science

⁴ Collaborative Innovation Center of Novel Software Technology and Industrialization

KEY WORDS: Vegetation Index, Light Use Efficiency, Gross Primary Production, Solar-induced Chlorophyll Fluorescence, Agriculture

ABSTRACT:

Over the last 40 years, the light use efficiency (LUE) model has become a popular approach for gross primary productivity (GPP) estimation in the carbon and remote sensing communities. Despite the fact that the LUE model provides a simple but effective way to approximate GPP at ecosystem to global scales from remote sensing data, when implemented in real GPP modelling, however, the practical form of the model can vary. By reviewing different forms of LUE model and their performances at ecosystem to global scales, we conclude that the relationships between LUE and optical vegetation active indicators (OVAIs, including vegetation indices and sun-induced chlorophyll fluorescence-based products) across time and space are key for understanding and applying the LUE model. In this work, the relationships between LUE and OVAIs are investigated at flux-tower scale, using both remotely sensed and simulated datasets. We find that i) LUE-OVAI relationships during the season are highly site-dependent, which is complexed by seasonal changes of leaf pigment concentration, canopy structure, radiation and V_{cmax} ; ii) LUE tends to converge during peak growing season, which enables applying pure OVAI-based LUE models without specifically parameterizing LUE and iii) Chlorophyll-sensitive OVAIs, especially machine-learning-based SIF-like signal, exhibits a potential to represent spatial variability of LUE during the peak growing season. We also show the power of time-series model simulations to improve the understanding of LUE-OVAI relationships at seasonal scale.

1. INTRODUCTION

Photosynthesis plays an essential role in global carbon cycle (Beer et al. 2010). Modelling gross primary productivity (GPP) quantifies the amount of total carbon fixation (prior to respiration) by terrestrial plants through photosynthesis (Running et al. 2004; Xiao et al. 2004). Remote sensing (RS) data hold a crucial and irreplaceable role in modelling GPP at multi spatio-temporal scales (Ollinger 2011). Originated from Monteith (1972), the light use efficiency (LUE) model has become a popular approach in the carbon and RS communities (Gitelson and Gamon 2015). Carbon assimilation is described by the LUE model as an integrated process of light absorption and carbon conversion through:

$$GPP = PAR \times fPAR \times LUE = APAR \times LUE \quad (1)$$

where PAR is photosynthetically active radiation (solar radiation around 400 – 700 nm), fPAR is the fraction of PAR absorbed by green vegetation and the product of PAR and fPAR is termed as APAR (absorbed PAR). Spatial temporal GPP variations are assumed to be driven by three key factors: PAR, fPAR and LUE. Eq. (1) provides a simple but effective way to approximate GPP at ecosystem to global scales from RS data (Zhang et al. 2018c).

When implemented in real GPP modelling, Eq. (1) has multiple forms. While PAR can be directly measured or inverted and

fPAR can be approximated using indicators based on optical remote sensing (including vegetation indices (VI) and solar-induced chlorophyll fluorescence (SIF), so-called optical vegetation active indicators (OVAIs)), the way of dealing with LUE differs. A variety of production efficiency models (PEMs) using the LUE concept have been proposed in the last decades based on different definitions and physical meanings of LUE (Gitelson and Gamon 2015).

A classic way that the concept of LUE is implemented in PEMs is assuming that actual LUE (LUE_{act}) can be scaled using maximum LUE (LUE_{max}) and scaling factors that relate to environmental stress:

$$GPP = APAR \times LUE_{act} = APAR \times LUE_{max} \times f(s_1, s_2, \dots) \quad (2)$$

where s_1 and s_2 are stress indicators such as vapour pressure deficit (Xiao et al. 2004) and soil moisture (Stocker et al. 2018) and f is scaling function. At regional to global scales, LUE_{max} is mapped according to plant functional type (Running et al. 2004; Zhang et al. 2017) or more advanced, through upscaling tower-based LUE_{max} , taking plant traits, climate and topology into account (Madani et al. 2014; Madani et al. 2017). Several long time-series global GPP products, including MODIS GPP product (Running et al. 2004) and VPM GPP (Zhang et al. 2017), have been produced based on Eq. (2). While LUE_{max} -based PEMs were commonly used for GPP estimation at regional to global

* Corresponding author

scales, at ecosystem level, simpler models that are only based on OVAIs have been proposed. For example, seasonal change of LUE has been found to be related to canopy chlorophyll in crops and the product of PAR and chlorophyll index was used to indicate GPP (Peng and Gitelson 2012; Peng et al. 2011). Similarly, Wu et al. (2010) proposed a VI-based LUE model, where VIs (including the normalized difference vegetation index, NDVI and the enhanced vegetation index, EVI) were used as LUE indicators at seasonal scale, and GPP can be therefore approximated by:

$$\text{GPP} = \text{APAR} \times \text{LUE} = \text{APAR} \times f(\text{OVAI}) \quad (3)$$

Since these pure OVAI-based PEMs have been shown to provide improved GPP estimations at ecosystem scales (Wagle et al. 2016; Wu et al. 2010), several recent studies have shown the potential of applying these models across different biomes and even at global scale. Without additional parameterization of LUE, Badgley et al. (2017) reported a near-universal linear relationship between near-infrared of vegetation (NIRv, the product of NDVI and near-infrared reflectance) and GPP across a wide range of biomes. Joiner et al. (2018) extended the application of Eq. (3) to global scale and showed its advantage over other state-of-the-art GPP estimations. These findings suggest OVAIs may carry important information on LUE across time and space and provide promising alternative solutions to estimate GPP at large scales.

Despite differ in formulations, all of the reviewed PEMs use the concept of LUE more or less. Different models have been used from time to time to estimate GPP and all of them have been reported to provide reasonable GPP estimations from ecosystem to global scales. Therefore, there could be potential links among different PEMs. As introduced in previous context, spatial-temporal variations of LUE are described in a variety of ways, which is the major difference among PEMs. In this sense, it is of primary importance to understand the spatio-temporal variability of LUE and its relationship to OVAIs, which could be key to further understand the fundamental basis and applicability of the proposed PEMs. In this context, the focus of the current study is to explore the relationship between LUE and OVAIs across time and space using both simulated and measured data, in order to better understand the potential links among different PEMs and to improve the use of LUE model in GPP estimation at ecosystem to global scales.

2. INTRODUCTION

2.1 FLUXNET 2015 dataset

We used monthly GPP and PAR data obtained from FLUXNET 2015 tier1 release (<http://fluxnet.fluxdata.org/data/download-data/>). GPP was estimated from net ecosystem exchange (NEE) using either day-time (DT) (Lasslop et al. 2010) or night-time (NT) (Reichstein et al. 2005) partitioning method. In order to reduce the uncertainty introduced by partitioning, we applied a filtering method following (Zhang et al. 2018d). Only data with difference between values from the two methods smaller than 20% or $2 \text{ g C m}^{-2} \text{ day}^{-1}$ were used. The average of DT and NT GPP was finally used for analysis. PAR was approximated from shortwave radiation data using a scaling factor of 0.48. Because there is still a gap between flux tower footprint and remote sensing pixel, only sites with coefficient of determination (R^2) between multi-year CSIF and GPP higher than 0.6 were used in order to reduce the impact of site heterogeneity. In total, 84 sites covering 9 different biomes were included in this study.

2.2 OVAIs from satellite remote sensing

In this study, five commonly used OVAIs for GPP estimation are used, including four VIs (NDVI, EVI, near-infrared reflectance of vegetation (NIRv) and MERIS terrestrial chlorophyll index (MTCI)) and one reproduced SIF-like product (continuous SIF, CSIF).

Site-specific NDVI, EVI were derived from MODIS VI product (MOD13A3, 1 km, monthly) and NIRv was calculated as the product of monthly-mean NDVI and near-infrared reflectance (provided in MOD13A3). MTCI data were downloaded from CEDA website (<http://data.ceda.ac.uk/neodc/mtci/data/global/>, monthly, $\sim 0.0416^\circ$).

SIF is a novel OVAI that is closely related to chlorophyll and has been used as GPP proxies at seasonal to global scales (Guanter et al. 2014; Zhang et al. 2014). Instead of using currently available raw SIF products (e.g. GOME-2 or OCO-2 SIF), this study used CSIF, a reproduced SIF-like signal, in tower-based analyses. CSIF is a machine learning (ML) product based on OCO-2 far-red SIF and MODIS visible and near-infrared (VNIR) reflectance (first four spectral bands, i.e. blue, green, red and NIR) as inputs (Zhang et al. 2018b). All-sky daily averaged CSIF from 2001 to 2014 was used in this study. Original 4-daily CSIF was resampled to monthly using the number of days in the month of interest contained by each 4-daily estimate as weight.

2.3 Time series radiative transfer and gas exchange simulations

In order to better understand the relationship between LUE and OVAIs at seasonal scale, we performed time-series simulations for several flux-tower sites using the Soil-Canopy-Observation of Photosynthesis and the Energy balance (SCOPE) model (Tol 2009). In this study, we used time-series SCOPE simulation data for 13 flux tower sites (Zhang et al. 2016). Specifically, leaf chlorophyll content (Cab) was inverted from MTCI, leaf area index (LAI) was derived from site-specific websites or RS-based product (MOD15A2) and meteorological data were recorded by flux tower measurements. Maximum carboxylation capacity (V_{cmax}), another key parameter that influences GPP simulation, was firstly set as biome-specific-seasonal-constant. Then seasonal-dynamic V_{cmax} inverted from in-situ GPP data (Zhang et al. 2018a) was used to better simulate GPP for US-Ha1 site. Detailed about this SCOPE-based dataset can be found in Zhang et al. (2016) and (Zhang et al. 2018a). Daily and monthly GPP, APAR and OVAIs were averaged from half-hourly or hourly simulations. Note that PAR absorbed by chlorophyll (APAR_{chl}), which was reported to be more closely related to photosynthesis, was used in all SCOPE-based analyses.

2.4 Linking LUE and OVAIs across time and space

According to Eq. (1), LUE is defined as the ratio between GPP and APAR. While APAR is an output of SCOPE simulations, it is generally calculated as the product of PAR and fPAR in real situations. Typically, a linear and robust correlation between fPAR and greenness vegetation index (VI) can be found at ecosystem level (Gitelson et al. 2014; Peng et al. 2011). Among all the VIs, NDVI and the enhanced vegetation index (EVI) are mostly commonly used to represent fPAR (Walther et al. 2016; Wang et al. 2017). Although EVI was reported to be better related to chlorophyll and more resistant to canopy background (Huete et al. 2002; Zhang et al. 2018c), its sensitivity to NIR reflectance, which is not directly related to fPAR but is sensitive to canopy structure (Knyazikhin et al. 2013), sun-sensor geometry and leaf

dry matter content (Verrelst et al. 2015), may induce uncertainties when it is used as a fPAR proxy across a variety of sites. Simulations from the SCOPE model help to illustrate this issue (Figure 1). Therefore, NDVI was finally selected as a robust fPAR proxy for all sites in this study.

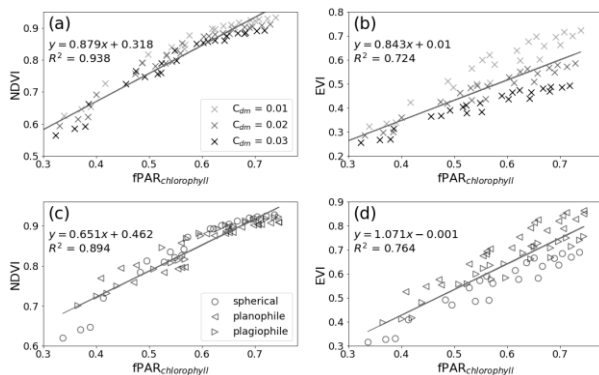


Figure 1. Simulated relationship between fPAR_{chlorophyll} and VI using inputs described in Table S1 (a and b for Case 1 and c and d for Case 2). PAR absorbed by chlorophyll was used to calculate fPAR_{chlorophyll}.

In most cases, a bias could be found for NDVI-fPAR linear relationship, i.e fPAR is proportional to NDVI subtracting a bias:

$$\text{fPAR} = k \times (\text{NDVI} - \text{bias}) \quad (4)$$

where the bias should be related to canopy background, which could be site-dependent, while k is determined by the Beer's Law, which should be ideally a constant and independent of biome type. In this study, we applied a similar strategy used in Zhang et al. (2018c) calculating site-specific bias using the intercept of the linear regression between apparent SIF yield (i.e. the ratio between CSIF and PAR) and NDVI (Figure 2).

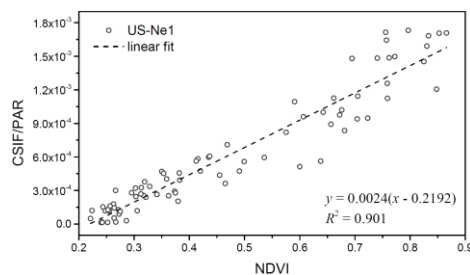


Figure 2. An example (US-Ne1 site) of using apparent SIFy (CSIF divided by PAR) to calculate site-specific bias of NDVI.

In this study, we first investigated the relationships between LUE and OVAIs at seasonal scale using both simulated and real data. Analysis based on SCOPE model were made on both daily and monthly basis while for real data, analysis was made at monthly scale. While the potential link between OVAIs and LUE at seasonal may help to illustrate the applicability of pure OVAI-based PEMs at single ecosystem level, for GPP estimations at larger (e.g. regional to global) scales, the inherent differences in the ability of carbon assimilation among different ecosystems should be also considered. For pure OVAI-based PEMs, this part of difference is represented by OVAIs (Joiner et al. 2018).

Therefore, we then analyzed the potential of different OVAIs to indicate inter-site LUE variations. Instead of using maximum LUE values for each site during the whole season, we calculated site-specific LUE only using data during un-stressed peak growing seasons, which were determined as the period within top 5% bins over multi-year GPP estimations. Note that impacts from potential environmental stress are expected to be avoided by the top 5% criteria.

3. RESULTS AND DISCUSSION

3.1 Relationship between LUE and OVAI at seasonal scale

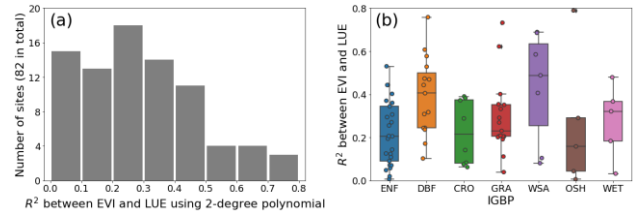


Figure 3. Correlation between EVI and LUE at seasonal scale for all flux tower sites used (a) and for different biomes (b). IGBP in (b) indicates different biome types of flux tower sites: evergreen needle leaf forest (ENF), deciduous broadleaf forest (DBF, including mixed forest sites), cropland (CRO), grassland (GRA), woody savanna (WSA, including savanna), open shrubland and wetland (WET).

Within the first step, we investigated the relationships between LUE and OVAIs at monthly scale on per-site basis based on FLUXNET 2015 dataset. Following Joiner et al. (2018), a two-degree polynomial was used to fit potential seasonal LUE-OVAI correlation for all sites. Figure 3 shows the derived relationship between LUE and EVI for 82 flux tower sites used. A strong site dependency can be found for seasonal LUE-EVI correlations. For most sites, a relatively weak LUE-EVI correlation (with R^2 lower than 0.5) could be found. For some sites, however, seasonal LUE and EVI are strongly correlated. In order to better understand the observed site-dependency of LUE-EVI correlation, we analyzed simulated data from SCOPE at monthly scale. Figure 4 shows the seasonal cycles of EVI and LUE for two sites showing contrasting LUE-EVI relationships based on both real and simulated data. It is shown by Figure 4 that results based on SCOPE simulations are overall consistent with those based on real data. A clear LUE seasonality, which is similar to the seasonal pattern of EVI, is found for US-Ha1 (Figure 4a), resulting in a strong LUE-EVI correlation for both real (Figure 4b) and simulated data (Figure 4c). For RU-Fyo site, however, no clear LUE seasonality is shown and seasonal LUE and EVI seem to be uncorrelated. The lower seasonal variability of simulated LUE than observed LUE could be due to seasonal-constant V_{cmax} assigned in simulations. We further used seasonal-dynamic V_{cmax} that inverted based on the gap between simulated GPP (with constant V_{cmax}) and flux tower-based GPP as input to better simulate seasonal LUE. Results (Figure 5) for US-Ha1 show that with a similar seasonal pattern of V_{cmax} , seasonal LUE and EVI exhibit a stronger linear correlation ($R^2 = 0.907$).

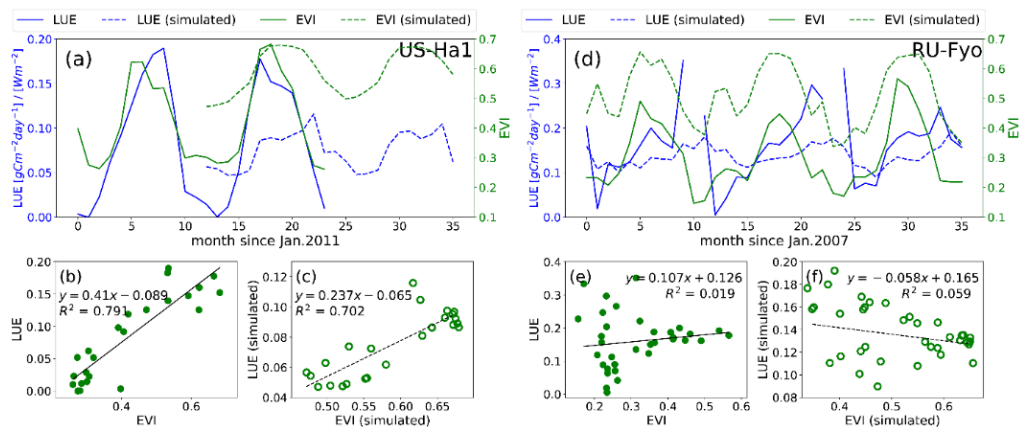


Figure 4. Time series (a, d) and scatter plots (b, c, e, f) showing contrasting relationships between monthly LUE and EVI at seasonal scale for US-Ha1 site (a-c, 2011-2013, deciduous broadleaf forest) and RU-Fyo site (d-f, 2007-2009, evergreen needleleaf forest). Results based on both real and simulated data are shown. Seasonal constant V_{cmax} values (57.7 and 62.5 for US-Ha1 and RU-Fyo, respectively) are used in SCOPE simulations.

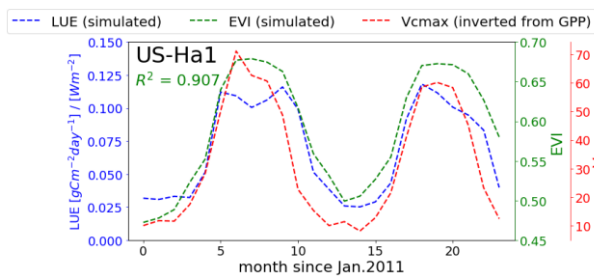


Figure 5. Simulated EVI and LUE seasonal cycles for US-Ha1 site with V_{cmax} inverted from GPP. R^2 is the coefficient of determination between monthly EVI and LUE, part of the LUE variability can be explained by NIR-sensitive (red-edge-sensitive) VIs;

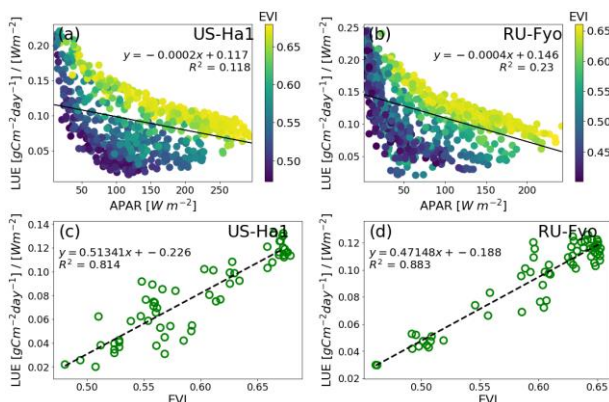


Figure 6. Simulated relationships between daily APAR and LUE during all seasons (a and b) and simulated LUE-EVI relationships with APAR between $130 W m^{-2}$ to $150 W m^{-2}$ (c and d) for US-Ha1 and RU-Fyo.

Despite the two sites are showing contrasting LUE-EVI relationships, the good consistency between results from real and simulated data makes it reasonable to discover possible reasons for the observed site-dependency of EVI-LUE relationship from SCOPE simulations. In SCOPE model, leaf-level LUE (i.e. photosynthesis quantum yield per APAR, ϕ_p) is mainly driven by the amount of APAR and V_{cmax} (van der Tol et al. 2014) (air temperature, which is also a seasonal-variable input of the simulations, has relatively weak influence on ϕ_p compared to APAR and V_{cmax}). Since results in Figure 4 are based on simulations with seasonal-constant V_{cmax} (57.7 and 62.5 for

US-Ha1 and RU-Fyo, respectively), APAR might be the most important factor that influences LUE. Figure 5a and Figure 5b show the simulated relationships between daily APAR and LUE for the two sites at different EVI levels across the whole simulation periods. It is shown that for both sites, APAR and LUE are negatively correlated at each EVI level. It can be also interpreted that for certain APAR level, higher EVI is accompanied with higher LUE, which is further illustrated by Figure 6c and Figure 6d. One possible reason for the close relationship between LUE and EVI could be their common sensitivity to canopy chlorophyll, which is directly related to electron transportation rate and dominates the spectral reflectance of VNIR range (Peng et al. 2011; Wang et al. 2017). However, the LUE-EVI relationship is further complexed at seasonal scale by seasonal change of APAR, especially in the presence of clear-cloudy sky conditions. Canopy level LUE is determined by ϕ_p of all leaves within the canopy. Consequently, canopy level of LUE is not only related to absolute value of canopy APAR, but is also determined by vertical distribution of APAR within the canopy, which is related to leaf chlorophyll content and canopy structure and can be further represented by EVI. Therefore, APAR and EVI jointly influence observed LUE at canopy level and LUE-EVI relationships across season is also influenced by seasonal change of APAR. Site-specific seasonal changes of PAR, Cab and LAI could jointly affect the observed seasonality of LUE, resulting in possible site-dependency of LUE-EVI correlation. Although a clear seasonal pattern of inverted V_{cmax} is found for US-Ha1, it should be noted that the V_{cmax} seasonality is determined by the gap between actual and modelled photosynthesis (GPP). Therefore, expect for seasonal change of V_{cmax} , other factors like imperfect approximations of actual Cab and LAI and limitations of physical photosynthesis model could also lead to a seasonality of the gap between EC-based and SCOPE-based GPP, which will further result in an inverted V_{cmax} seasonality.

3.2 Variability of LUE and OVAs across sites and biomes

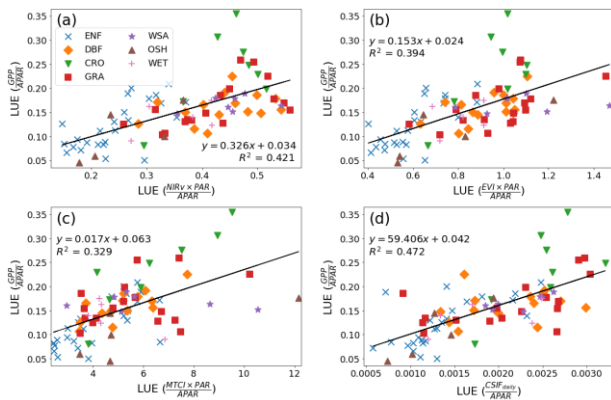


Figure 7. Relationships between LUE based on GPP-EC and LUE based on different PEMs during peak growing seasons across flux tower sites.

While the potential links between OVAs and LUE at seasonal scale lay the fundamental basis for applying pure OVAI-based PEMs at single system, the ability of OVAs to indicate LUE among different ecosystems determines the applicability of these PEMs at large scales. Figure 7 shows the relationships between LUE and 4 chlorophyll-sensitive OVAs, NIRv, EVI, MTCI and CSIF. It can be interpreted that regardless of plant functional types (PFTs), all of the OVAs show moderate strong correlations to LUE. Among the 4 studied OVAs, LUE based on CSIF show the strongest relationship to LUE ($R^2 = 0.472$) while MTCI shows the weakest ($R^2 = 0.329$). NIRv and EVI show similar performances to track inter-site LUE differences (with R^2 of 0.421 and 0.394 for NIRv and EVI, respectively). We then analyzed the potential biome-dependency of LUE-OVAI relationship (only results for CSIF is shown here). Figure 8a shows the variability of LUE during peak growing seasons according to different biomes. Figure 8b shows the variation of GPP-CSIF ratio, which is also the ratio between LUE and LUE_r , among different biomes. On average, cropland (CRO) exhibits the highest LUE while evergreen needleleaf forest (ENF) and open shrubland (OSH) gains the lowest. As for the GPP-SIF ($LUE-LUE_r$) ratio, higher values are found in both ENF and CRO.

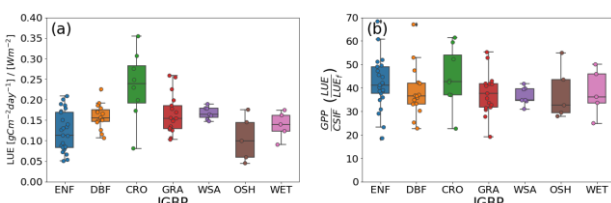


Figure 8. LUE (a) and the ratio between GPP and CSIF (b) according to biome types.

All of the 4 OVAs used, including three VIs and one SIF-like signal, are shown to be related to LUE across different sites. For the three VIs (i.e. NIRv, EVI and MTCI) used in Figure 8, they are sensitive to NIR reflectance, which is also sensitive to LAI. NIR reflectance-sensitive VIs have been reported to be closely related to total canopy chlorophyll (the product of LAI and C_{ab}) (Peng et al. 2011). Furthermore, at regional scale, NIR reflectance has been shown to be also related to foliar nitrogen content (Ollinger et al. 2008), although the physical basis behind the relationship is controversial (Knyazikhin et al. 2013). On this basis, the positive correlations between LUE and NIR reflectance-sensitive VIs are expected to be explained by their common sensitivity to canopy chlorophyll and nitrogen content.

Similarly, CSIF is also closely related to NIR reflectance, not only because NIR reflectance is one of the inputs of the ML approach, but also due to the similarity between canopy scattering of far-red SIF and NIR photons (Liu et al. 2018; Yang and van der Tol 2018). Additional information that CSIF carries on LUE may also come from the closer relationship between SIF and V_{cmax} (Zhang et al. 2014; Zhang et al. 2018a) or visible band reflectance.

On per biome basis, LUE shows significant difference among biomes (with $p < 0.001$ in ANOVA test) (Figure 8a). In contrast, GPP-CSIF ratio, which is a proxy of LUE-OVAI relationship, shows no significant biome dependency (with $p = 0.742$ in ANOVA test) (Figure 8b). This indicates that most biome-dependency of LUE can be explained and represented by OVAs. Yet ENF and CRO still show a higher GPP-CSIF ratio than other biomes ($p = 0.079$ in ANOVA test when ENF and CRO are grouped together and compared with other biomes). Canopy scattering of SIF (and also NIR photons) in a coniferous canopy is stronger than that in a broadleaf canopy with same LAI (Rautiainen et al. 2009). Besides, needles generally consist higher dry matter content than leaves, resulting in a lower single scattering albedo at far-red spectral range (Knyazikhin et al. 2013). Therefore, CSIF in ENF could be lower due to a stronger re-absorption, which is a radiative transfer artifact and not related to GPP. As for crop sites, higher GPP-SIF ratio could be due to higher electron use efficiency of C4 crops (Guan et al. 2016), which cannot be presented by OVAs (Liu et al. 2017; Wood et al. 2017).

3.3 Implications for GPP estimation at ecosystem to global scales

At ecosystem scale, pure OVAI-based PEMs have been used to estimate GPP. Results in Section 3.1 show that LUE-OVAI relationship at seasonal scale is complexed by the seasonal changes of APAR and V_{cmax} , which could be site-dependent and leads to contrasting seasonal LUE-OVAI relationships. The site dependency of LUE-OVAI relationship seems to exist for all biomes (Figure 3b), but DBF sites generally show higher R^2 values between seasonal LUE and OVAI than ENF sites. This may be due to the fact that DBF exhibits a stronger seasonal change of canopy and leaf structure, which may result in a clear LUE seasonality that is similar to canopy greenness (Wang et al. 2017). It should be noted that this study used NDVI subtracting a bias as a robust $fPAR_{chl}$ proxy at seasonal scale across different sites (Figure 2), but NDVI may be more closely related to $fPAR_{total}$ in real situations (Zhang et al. 2018c). Therefore, the seasonality of observed LUE seasonality based on real data may be partly due to the potential seasonality of $fPAR_{chl}$ - $fPAR_{total}$ ratio. As it is challenging to separate $fPAR_{chl}$ from $fPAR_{total}$ using OVAI, this part of change was regarded as LUE change in this study.

While Eq. (3) uses OVAI to represent LUE, in other pure OVAI-based PEMs, LUE is not specifically parameterized and GPP is directly represented by the product of PAR and a selected chlorophyll-sensitive OVAI (e.g. chlorophyll index and NIRv). On one hand, chlorophyll-sensitive OVAs may carry information on LUE, as suggested by Figure 3 and Figure 8. On the other hand, the relatively good performances of these models may be also due to the fact that LUE can be quite stable for certain ecosystem during peak growing seasons (Gitelson et al. 2018). This is also illustrated by Figure 4, where LUE for both selected sites are converged when EVI is high. It can be interpreted that most GPP variability during peak growing seasons can be captured by APAR, which can be represented by

the product of PAR and OVAI. Based on the fact that GPP during peak growing season makes the majority of annual GPP, for single ecosystem, pure OVAI-based PEMs may show good performances with or without specific parameterization of LUE using OVAI. In this context, understanding the spatial variability of LUE during peak growing season becomes even more crucial for GPP estimation at regional to global scales.

Classic LUEmax-based PEMs use pre-defined LUEmax for different biomes. A major shortcoming for these PEMs is that LUEmax shows a relatively large variability within single PFT (Madani et al. 2014) (also shown by Figure 8a). Instead of using pre-defined biome-specific LUEmax, Madani et al. (2017) proposed to use spatially continuous LUE during unstressed peak growing seasons upscaled from flux tower-based LUE. More precisely, they defined the newly proposed LUE as optimum LUE (LUEopt, i.e. LUE under optimal environmental conditions). Results presented in Figure 8 show the great potential of chlorophyll-sensitive OVAIs to representing the spatial heterogeneity of LUEopt. The positive correlations between LUEopt and OVAIs also explain the observed convergence of EVI-based LUE among a variety of biomes (Zhang et al. 2018c) and the near-universal NIRv-GPP relationships across different flux tower sites (Badgley et al. 2017). Among the four studied chlorophyll-sensitive OVAIs, CSIF-based LUE shows the highest correlation with actual LUE. Madani et al. (2017) reported that GOME-2 SIF can explain 36.3% of LUEopt variability. Results in Figure 7d show the potential of applying ML-based SIF-like signal in mapping spatially continuous LUEopt, especially after canopy structure effects in SIF (and also in spectral reflectance) and C3-C4 difference are properly modeled.

4. SUMMARY

In this study, we investigated the relationships between LUE and OVAIs across time and space, in order to better understand the fundamental basis of different PEMs. Specifically, we found that:

1. LUE-OVAI relationships during the season were highly site-dependent, which was complexed by seasonal changes of leaf pigment concentration, canopy structure, radiation and V_{cmax} ;
2. LUE tended to converge during peak growing season, which enabled applying pure OVAI-based PEMs without specifically parameterizing LUE;
3. Chlorophyll-sensitive OVAIs, especially ML-based SIF-like signal, showed great potential to represent spatial heterogeneity of LUE during peak growing season.

We also showed the power of time-series model simulations to improve the understanding of LUE-OVAI relationships at seasonal scale. At single ecosystem level, single chlorophyll-sensitive OVAI may capture most information of photosynthesis-related vegetation activity. At regional to global scales, mapping spatially-continuous LUE is most important in GPP estimation. Canopy structure effects in OVAIs and other physiological factors such as C3-C4 differences should be considered when relating LUE and OVAIs at large scales. It should be noted that the influence of environmental stress on LUE and LUE-OVAI relationship is not specifically discussed in this study, which needs further investigations.

REFERENCES

Badgley, G., Field, C.B., & Berry, J.A. (2017). Canopy near-infrared reflectance and terrestrial photosynthesis. *Science Advances*, 3, e1602244

Beer, C., Reichstein, M., Tomelleri, E., Ciais, P., Jung, M., Carvalhais, N., Rödenbeck, C., Arain, M.A., Baldocchi, D., & Bonan, G.B. (2010). Terrestrial gross carbon dioxide uptake: global distribution and covariation with climate. *Science*, 329, 834-838

Damm, A., Guanter, L., Paul-Limoges, E., van der Tol, C., Hueni, A., Buchmann, N., Eugster, W., Ammann, C., & Schaepman, M.E. (2015). Far-red sun-induced chlorophyll fluorescence shows ecosystem-specific relationships to gross primary production: An assessment based on observational and modeling approaches. *Remote Sensing of Environment*, 166, 91-105

Gitelson, A.A., Arkebauer, T.J., & Suyker, A.E. (2018). Convergence of daily light use efficiency in irrigated and rainfed C3 and C4 crops. *Remote Sensing of Environment*, 217, 30-37

Gitelson, A.A., & Gamon, J.A. (2015). The need for a common basis for defining light-use efficiency: Implications for productivity estimation. *Remote Sensing of Environment*, 156, 196-201

Gitelson, A.A., Peng, Y., & Huemmrich, K.F. (2014). Relationship between fraction of radiation absorbed by photosynthesizing maize and soybean canopies and NDVI from remotely sensed data taken at close range and from MODIS 250m resolution data. *Remote Sensing of Environment*, 147, 108-120

Guan, K., Berry, J.A., Zhang, Y., Joiner, J., Guanter, L., Badgley, G., & Lobell, D.B. (2016). Improving the monitoring of crop productivity using spaceborne solar-induced fluorescence. *Glob Chang Biol*, 22, 716-726

Guanter, L., Zhang, Y., Jung, M., Joiner, J., Voigt, M., Berry, J.A., Frankenberg, C., Huete, A.R., Zarco-Tejada, P., & Lee, J.-E. (2014). Global and time-resolved monitoring of crop photosynthesis with chlorophyll fluorescence. *Proceedings of the National Academy of Sciences*, 111, E1327-E1333

Huete, A., Didan, K., Miura, T., Rodriguez, E.P., Gao, X., & Ferreira, L.G. (2002). Overview of the radiometric and biophysical performance of the MODIS vegetation indices. *Remote Sensing of Environment*, 83, 195-213

Joiner, J., Yoshida, Y., Zhang, Y., Duveiller, G., Jung, M., Lyapustin, A., Wang, Y., & Tucker, C. (2018). Estimation of Terrestrial Global Gross Primary Production (GPP) with Satellite Data-Driven Models and Eddy Covariance Flux Data. *Remote Sensing*, 10, 1346

Knyazikhin, Y., Schull, M.A., Stenberg, P., Möttus, M., Yang, Y., Marshak, A., Carmona, P.L., Kaufmann, R.K., & Lewis, P. (2013). Hyperspectral remote sensing of foliar nitrogen content. *Proceedings of the National Academy of Sciences*, 110, E185-E192

Lasslop, G., Reichstein, M., Papale, D., Richardson, A.D., Arneth, A., Barr, A., Stoy, P., & Wohlfahrt, G. (2010). Separation of net ecosystem exchange into assimilation and respiration using a light response curve approach: critical issues and global evaluation. *Glob Chang Biol*, 16, 187-208

Liu, L., Guan, L., & Liu, X. (2017). Directly estimating diurnal changes in GPP for C3 and C4 crops using far-red sun-induced chlorophyll fluorescence. *Agricultural and Forest Meteorology*, 232, 1-9

- Liu, X., Guanter, L., Liu, L., Damm, A., Malenovsky, Z., Rascher, U., Peng, D., Du, S., & Gastellu-Etchegorry, J.-P. (2018). Downscaling of solar-induced chlorophyll fluorescence from canopy level to photosystem level using a random forest model. *Remote Sensing of Environment*
- Madani, N., Kimball, J.S., Affleck, D.L., Kattge, J., Graham, J., Bodegom, P.M., Reich, P.B., & Running, S.W. (2014). Improving ecosystem productivity modeling through spatially explicit estimation of optimal light use efficiency. *Journal of Geophysical Research: Biogeosciences*, 119, 1755-1769
- Madani, N., Kimball, J.S., & Running, S.W. (2017). Improving Global Gross Primary Productivity Estimates by Computing Optimum Light Use Efficiencies Using Flux Tower Data. *Journal of Geophysical Research: Biogeosciences*, 122, 2939-2951
- Ollinger, S.V. (2011). Sources of variability in canopy reflectance and the convergent properties of plants. *New Phytol*, 189, 375-394
- Ollinger, S.V., Richardson, A.D., Martin, M.E., Hollinger, D.Y., Froelking, S.E., Reich, P.B., Plourde, L.C., Katul, G.G., Munger, J.W., & Oren, R. (2008). Canopy nitrogen, carbon assimilation, and albedo in temperate and boreal forests: Functional relations and potential climate feedbacks. *Proceedings of the National Academy of Sciences*, 105, 19336-19341
- Peng, Y., & Gitelson, A.A. (2012). Remote estimation of gross primary productivity in soybean and maize based on total crop chlorophyll content. *Remote Sensing of Environment*, 117, 440-448
- Peng, Y., Gitelson, A.A., Keydan, G., Rundquist, D.C., & Moses, W. (2011). Remote estimation of gross primary production in maize and support for a new paradigm based on total crop chlorophyll content. *Remote Sensing of Environment*, 115, 978-989
- Rautiainen, M., Möttöus, M., & Stenberg, P. (2009). On the relationship of canopy LAI and photon recollision probability in boreal forests. *Remote Sensing of Environment*, 113, 458-461
- Reichstein, M., Falge, E., Baldocchi, D., Papale, D., Aubinet, M., Berbigier, P., Bernhofer, C., Buchmann, N., Gilmanov, T., & Granier, A. (2005). On the separation of net ecosystem exchange into assimilation and ecosystem respiration: review and improved algorithm. *Glob Chang Biol*, 11, 1424-1439
- Running, S.W., Nemani, R.R., Heinsch, F.A., Zhao, M., Reeves, M., & Hashimoto, H. (2004). A continuous satellite-derived measure of global terrestrial primary production. *AIBS Bulletin*, 54, 547-560
- Ryu, Y., Jiang, C., Kobayashi, H., & Detto, M. (2018). MODIS-derived global land products of shortwave radiation and diffuse and total photosynthetically active radiation at 5 km resolution from 2000. *Remote Sensing of Environment*, 204, 812-825
- Stocker, B.D., Zscheischler, J., Keenan, T.F., Prentice, I.C., Penuelas, J., & Seneviratne, S.I. (2018). Quantifying soil moisture impacts on light use efficiency across biomes. *New Phytol*, 218, 1430-1449
- Tol, C.v.d. (2009). An integrated model of soil-canopy spectral radiances, photosynthesis, fluorescence, temperature and energy balance. *Biogeosciences*, 6, 3109-3129
- van der Tol, C., Berry, J.A., Campbell, P.K.E., & Rascher, U. (2014). Models of fluorescence and photosynthesis for interpreting measurements of solar-induced chlorophyll fluorescence. *Journal of Geophysical Research: Biogeosciences*, 119, 2312-2327
- Verrelst, J., Rivera, J.P., van der Tol, C., Magnani, F., Mohammed, G., & Moreno, J. (2015). Global sensitivity analysis of the SCOPE model: What drives simulated canopy-leaving sun-induced fluorescence? *Remote Sensing of Environment*, 166, 8-21
- Wagle, P., Zhang, Y., Jin, C., & Xiao, X. (2016). Comparison of solar-induced chlorophyll fluorescence, light-use efficiency, and process-based GPP models in maize. *Ecological Applications*, 26, 1211-1222
- Walther, S., Voigt, M., Thum, T., Gonsamo, A., Zhang, Y., Kohler, P., Jung, M., Varlagin, A., & Guanter, L. (2016). Satellite chlorophyll fluorescence measurements reveal large-scale decoupling of photosynthesis and greenness dynamics in boreal evergreen forests. *Glob Chang Biol*, 22, 2979-2996
- Wang, S., Zhang, L., Huang, C., & Qiao, N. (2017). An NDVI-Based Vegetation Phenology Is Improved to be More Consistent with Photosynthesis Dynamics through Applying a Light Use Efficiency Model over Boreal High-Latitude Forests. *Remote Sensing*, 9, 695
- Wood, J.D., Griffis, T.J., Baker, J.M., Frankenberg, C., Verma, M., & Yuen, K. (2017). Multiscale analyses of solar-induced fluorescence and gross primary production. *Geophysical Research Letters*, 44, 533-541
- Wu, C., Niu, Z., & Gao, S. (2010). Gross primary production estimation from MODIS data with vegetation index and photosynthetically active radiation in maize. *Journal of Geophysical Research*, 115
- Xiao, X., Hollinger, D., Aber, J., Goltz, M., Davidson, E.A., Zhang, Q., & Moore, B. (2004). Satellite-based modeling of gross primary production in an evergreen needleleaf forest. *Remote Sensing of Environment*, 89, 519-534
- Yang, P., & van der Tol, C. (2018). Linking canopy scattering of far-red sun-induced chlorophyll fluorescence with reflectance. *Remote Sensing of Environment*, 209, 456-467
- Zhang, Y., Guanter, L., Berry, J., Van der Tol, C., Yang, X., Tang, J., & Zhang, F. (2016). Model-based analysis of the relationship between sun-induced chlorophyll fluorescence and gross primary production for remote sensing applications. *Remote Sensing of Environment*, 187
- Zhang, Y., Guanter, L., Berry, J.A., Joiner, J., van der Tol, C., Huete, A., Gitelson, A., Voigt, M., & Kohler, P. (2014). Estimation of vegetation photosynthetic capacity from space-based measurements of chlorophyll fluorescence for terrestrial biosphere models. *Glob Chang Biol*, 20, 3727-3742
- Zhang, Y., Guanter, L., Joiner, J., Song, L., & Guan, K. (2018a). Spatially-explicit monitoring of crop photosynthetic capacity

through the use of space-based chlorophyll fluorescence data. *Remote Sensing of Environment*, 210, 362-374

Zhang, Y., Joiner, J., Alemohammad, S.H., Zhou, S., & Gentine, P. (2018b). A global spatially Continuous Solar Induced Fluorescence (CSIF) dataset using neural networks. *Biogeosciences Discussions*, 1-34

Zhang, Y., Xiao, X., Wolf, S., Wu, J., Wu, X., Gioli, B., Wohlfahrt, G., Cescatti, A., van der Tol, C., & Zhou, S. (2018c). Spatio-temporal Convergence of Maximum Daily Light-Use Efficiency Based on Radiation Absorption by Canopy Chlorophyll. *Geophysical Research Letters*

Zhang, Y., Xiao, X., Wu, X., Zhou, S., Zhang, G., Qin, Y., & Dong, J. (2017). A global moderate resolution dataset of gross primary production of vegetation for 2000–2016. *Scientific data*, 4, 170165

Zhang, Y., Xiao, X., Zhang, Y., Wolf, S., Zhou, S., Joiner, J., Guanter, L., Verma, M., Sun, Y., Yang, X., Paul-Limoges, E., Gough, C.M., Wohlfahrt, G., Gioli, B., van der Tol, C., Yann, N., Lund, M., & de Grandcourt, A. (2018d). On the relationship between sub-daily instantaneous and daily total gross primary production: Implications for interpreting satellite-based SIF retrievals. *Remote Sensing of Environment*, 205, 276-289